Carbohydrate Polymers 87 (2012) 564–573

Contents lists available at ScienceDirect

Carbohydrate Polymers

journal homepage: www.elsevier.com/locate/carbpol

Preparation and characterization of cellulose nanocrystals from rice straw

Ping Lu, You-Lo Hsieh*

Fiber and Polymer Science, University of California, Davis, CA 95616, USA

ARTICLE INFO

Article history:
Received 8 July 2011
Received in revised form 4 August 2011
Accepted 9 August 2011
Available online 16 August 2011

Keywords:
Cellulose nanocrystals (CNCs)
Ultra-fine fibers
Self-assembly
Rice straw
Sulfuric acid hydrolysis

ABSTRACT

Pure cellulose have been isolated from rice straw at 36% yield and hydrolyzed (64% H_2SO_4, 8.75 mL/g, 45 °C) for 30 and 45 min to cellulose nanocrystals (CNCs), i.e., CNC30 and CNC45, respectively. CNC45 was smaller (11.2 nm wide, 5.06 nm thick and 117 nm long) than CNC30 (30.7 nm wide, 5.95 nm thick and 270 nm long). Freeze–drying of diluted CNC suspensions showed both assembled into long fibrous structures: ultra-fine fibers (~400 nm wide) from CNC45 and 1–2 μm wide broad ribbons interspersed with CNC clusters from CNC30. The self-assembled fibers from CNC30 and CNC45 were more highly crystalline (86.0% and 91.2%, respectively) and contained larger crystallites (7.36 nm and 8.33 nm, respectively) than rice straw cellulose (61.8%, 4.42 nm). These self-assembled fibers had essentially nonporous or macroporous structures with the CNCs well aligned along the fiber axis. Furthermore, the self-assembled ultra-fine fibers showed extraordinary structural stability, withstanding vigorous shaking and prolong stirring in water.

1. Introduction

In plant cells, cellulose chains are synthesized and assembled into highly organized fibrillar structures with lateral dimensions ranging from 2 to 20 nm and crystallinities from 65 to 95%, depending on their origin (Habibi, Lucia, & Rojas, 2010; Ishii, Saito, & Isogai, 2011; Lu & Hsieh, 2010; Paakko et al., 2007). These highly crystalline cellulose fibrils represent the main structural component, along with hemicellulose and lignin, of plant cell walls and are responsible for their high strength (Li & Renneckar, 2011). Various approaches such as acid hydrolysis (Roman & Gray, 2005), enzymatic digestion (Paakko et al., 2007), and oxidation (Okita, Fujisawa, Saito, & Isogai, 2010) combined with mechanical disintegration (Abe, Iwamoto, & Yano, 2007; Uetani & Yano, 2011) have been reported to derive cellulose fibrils from a variety of sources. In controlled acid hydrolysis with either sulfuric or hydrochloric acid, cellulose chains in the less ordered or amorphous domains are more easily accessed and preferentially decomposed, leaving the crystalline domains intact (Stephens, Whitmore, Morris, & Bier, 2008). These highly crystalline cellulose solids are rod-shaped and have been commonly referred to as cellulose nanocrystals (CNCs) or cellulose nanowiskers in the literature. CNCs from controlled sulfuric acid hydrolysis are typically 5–30 nm wide and 0.1–2 μm long (Elazzouzi-Hafraoui et al., 2008) and contain negatively charged sulfate groups on their surface to be aqueous dispersible (Jiang, Esker, & Roman, 2010; Winter et al., 2010). CNCs have extraordinary bending strength and modulus, estimated to be ~10 GPa and 150 GPa, respectively, that are comparable in magnitude to those of carbon nanotubes (Iwamoto, Kai, Isogai, & Iwata, 2009), low thermal expansion coefficient as well as high surface reactivity (Habibi et al., 2010). Derived from readily available cellulose, the nature's most abundant polymer, CNCs have the unparallel potentials the natural nanoelements at the cutting-edge of materials science. Reports of CNC applications have included reinforcing nanofillers in "green" nanocomposites (Cao, Habibi, & Lucia, 2009; Goetz, Foston, Mathew, Oksman, & Ragauskas, 2010; Habibi et al., 2008; Lu & Hsieh, 2009; Magalhaes, Cao, & Lucia, 2009; Olsson et al., 2010; Peresin, Habibi, Zoppe, Pawlak, & Rojas, 2010; Qi, Cai, Zhang, & Kuga, 2009; Siqueira, Bras, & Dufresne, 2010; Zoppe, Peresin, Habibi, Venditti, & Rojas, 2009) as well as other nanotechnology applications including surface coating materials(Ahola, Salmi, Johansson, Laine, & Osterberg, 2008; Mesquita, Donnici, & Pereira, 2010)and carriers for medicines (Dong & Roman, 2007; Dugan, Gough, & Eichhorn, 2010; Mahmoud et al., 2010).

Rice is the largest cereal crop in the world. Rice straw represents around 45% of the volume in rice production, producing the largest quantity of crop residue. As rice straw is a marginal feed compared to other cereal grain straw and a problematic fuel source due to high ash generation, exploring more viable options to utilize rice straw is pressing, particularly as an environmental concern. With its compositions of cellulose (38.3%), hemicellulose (31.6%), lignin (11.8%) and silica (18.3%)(Hessien, Rashad, Zaky, Abdel-Aal, & El-Barawy, 2009), rice straw is the most available cellulose source from agricultural crop residues in the world. To date, there have been

* Corresponding author. Tel.: +1 530 752 0843; fax: +1 530 752 7584.
E-mail address: ylhsieh@ucdavis.edu (Y.-L. Hsieh).

0144-8617/$ – see front matter © 2011 Elsevier Ltd. All rights reserved.
doi:10.1016/j.carbpol.2011.08.022

few studies on isolation and utilization of cellulose from rice straw. Deriving CNCs from rice straw cellulose has not been reported.

This study was to isolate cellulose from rice straw, derive CNCs from rice straw cellulose and gain insight into the structure of rice straw CNCs. High quality cellulose was isolated by streamlining and optimizing extraction and dissolution conditions to remove wax, lignin, hemicellulose and silica in a step-wise fashion. The resultant cellulose was hydrolyzed to CNCs by sulfuric acid. The dimensions as well as surface, pore and crystalline structures and aqueous stability of assembled CNCs as related to the levels of hydrolysis and the freeze–drying process were characterized in detail and compared to the cotton CNCs from our previous study (Lu & Hsieh, 2009, 2010).

2. Experimental

2.1. Materials

Rice straw (Calrose variety) used in this study was collected from 2009 harvest in the Sacramento valley in northern California. Sodium chlorite ($NaClO_2$, 80%, Fluka), acetic acid glacial (CH_3COOH, 99.7%, ACS GR, EMD) and potassium hydroxide (KOH, 85%, EM Science) for separation of cellulose from rice straw and sulfuric acid (H_2SO_4, 95–98%, ACS GR, EMD) for hydrolysis were used as received without further purification. All water used was purified by Milli-Q plus water purification system (Millipore Corporate, Billerica, MA).

2.2. Isolation of cellulose fibers (CFs) from rice straw

The non-cellulosic components in rice straw were removed to isolate cellulose by incorporating and streamlining procedures reported for varied biomass sources (Abe et al., 2007; Abe & Yano, 2010; Sun, Sun, Zhao, & Sun, 2004). Rice straw was thoroughly washed 3–4 times with warm tap water to remove dirt and aqueous soluble substances, followed by prolonged (about one week) air drying. The dryclean rice straw was milled (Thomas-Wiley Laboratory Mill model 4, Thomas Scientific, USA) to pass through a 60-mesh screen. Rice straw powder (30 g) was first extracted with 2:1, v/v toluene/ethanol(450 mL) mixture for 20 h to remove wax, pigments and oils, followed by oven-drying at 55 °C for 24 h. The dewaxed powder was then immersed in 1.4% acidified $NaClO_2$ (1000 mL), with pH adjusted to 3.0–4.0 by CH_3COOH, at 70 °C for 5 h to dissolve lignin. After quenching the reaction with ice and decanting the excess liquid, the light yellow solid was washed with copious amount of water until filtrate becoming neutral. Hemicellulose and silica in the delignified powder were leached with 600 mL 5% KOH at room temperature for 24 h and then at 90 °C for 2 h. The white cellulose powder was centrifuged and washed with copious amount of water until filtrate reached neutral. The aqueous sample suspension (~300 mL) was quickly frozen by pouring liquid nitrogen (N_2) into the sample container and then freeze–dried (FreeZone 1.0 L Benchtop Freeze Dry System, Labconco, Kansas City, MO) to remove water.

2.3. Preparation of cellulose nanocrystal fibers

Cellulose isolated from rice straw was hydrolyzed using 64–65 wt% sulfuric acid at an 8.75 mL/g acid-to-cellulose ratio as previously reported for softwood pulp (Dong & Roman, 2007; Roman & Gray, 2005), and at a temperature of 45 °C for 30 or 45 min. Acid hydrolysis was stopped by diluting with 10-fold ice water. The resulting cellulose nanocrystal gel was washed once, centrifuged at 5000 rpm for 25 min at 10 °C, and then dialyzed with regenerated cellulose dialysis membranes with 12–14 kDa molecular weight cut off (Fisherbrand, Pittsburgh, PA) against ultra-pure water (Millipore Milli-Q UF Plus) until reaching neutral pH. The suspension was sonicated (Branson ultrasonic processor model 2510, Danbury, CT) in an ice bath for 30 min, and then filtered (Whatman 541, Maidstone, Kent, England) to remove large pieces of aggregates. The CNC suspension at about 0.06 wt%was quickly frozen by pouring liquid nitrogen into the sample container and freeze–dried overnight to remove water. The dried product was stored under vacuum for the following characterizations.

2.4. Characterization

2.4.1. Fourier transform infrared spectroscopy (FTIR)

FTIR Spectra were measured using a Thermo Nicolet 6700 spectrometer (Thermo Fisher Scientific, USA) at ambient conditions. Samples were analyzed by grinding with KBr (1:100, w/w) and pressing into transparent pellets. The spectra were collected in the transmittance mode from an accumulation of 128 scans at a 4 cm^{-1} resolution over 4000–400 cm^{-1} range.

2.4.2. Optical and polarized light microscopy

Dry particulates and aqueous suspensions were observed under a Leica DM2500 optical microscope at 400 magnification with or without polarized filters.

2.4.3. Scanning electron microscopy (SEM)

The microstructures and surface morphologies were examined by a field emission scanning electron microscope (FE-SEM) (XL 30-SFEG, FEI/Philips, USA). The samples were mounted on aluminum stubs with conductive carbon tape and sputtered with gold under vacuum at 20 mA for 2 min (Bio-Rad SEM coating system). The samples were observed and imaged at an 8-mm working distance and 5-kV accelerating voltage. The fiber diameters were determined from more than 200 individual fibers by an image analyzer (analySIS FIVE, Soft Imaging System GmbH, Munster, Germany). The statistical analysis was performed using Origin Pro 8 SR2 and the mean, standard deviation and percent of coefficient of variation (%CV) were reported.

2.4.4. Energy-dispersive X-ray spectroscopy (EDS)

Sulfur mapping was conducted using the EDS (EDAX, AMETEK, Inc.) adjunct to the SEM at a spot size of 5 and magnification of 5000 with a 5-kV accelerating voltage and a 5-mm working distance (the exact focal plane of X-ray) for around 30 min.

2.4.5. Transmission electron microscopy (TEM)

To image CNCs, a drop of 10 μL diluted CNC suspension (0.005, w/w%) after dialysis and filtration was deposited onto glow-discharged carbon-coated TEM grids (300-mesh copper, formvar-carbon, Ted Pella Inc., Redding, CA) and the excess liquid was removed by blotting with a filter paper after 2 min. The specimens were then negatively stained with 2% uranyl acetate solution for 2 min, blotted with a filter paper to remove excess stain solution and allowed to dry at ambient condition. The samples were observed using a Philip CM12 transmission electron microscope operated at a 100 kV accelerating voltage. To image the freeze–dried CNCs, the samples were added onto the TEM grids by contacting grids, then blowing away the loose samples with compressed air. The samples were directly observed without staining using the same set-up as above. The diameter and size distribution of CNCs were measured on around 200 representative CNCs using analySIS FIVE and Origin Pro software.

2.4.6. Wide-angel X-ray diffraction (XRD)

The overall crystalline phases of samples were determined by XRD measurement on a Scintag XDS 2000 powder diffractometer. XRD samples were prepared by pressing CNCs between two glass slides into flatten sheets. Radial scans of intensity were recorded

at ambient condition over scattering 2θ angles from 5° to 40° (step size = 0.02°, scanning rate = 2 s/step) using a Ni-filtered Cu Kα radiation (λ = 1.5406 Å), an operating voltage of 45 kV, and a filament current of 40 mA. Crystallinity index (CrI) of each sample was calculated by referring to diffraction intensity of crystalline and amorphous regions using the following empirical equation (Segal, Creely, Martin, & Conrad, 1959) (1):

$$CrI = \frac{I_{200} - I_{am}}{I_{200}} \times 100 \quad (1)$$

where I_{200} is the peak intensity at plane (2 0 0) (2θ = 22.6°), and I_{am} is the minimum intensity at the valley between plane (2 0 0) and (1 1 0) (2θ = 18.7°).

Crystal size was estimated using the Scherrer Eq. (2) and peak fitting process of the diffraction profile for the Scherrer equation calculation was done in PeakFit v4.12, using Lorentz distribution with major diffraction peak positions fixed (Elazzouzi-Hafraoui et al., 2008; Yu, Chen, Men, & Hwang, 2009).

$$D_{hkl} = \frac{0.9\lambda}{\beta_{1/2} \cos\theta} \quad (2)$$

where D_{hkl} is the crystal dimension perpendicular to the diffracting planes with Miller indices of *hkl*, λ is the wavelength of X-ray radiation (λ = 1.5406 Å) and $\beta_{1/2}$ is the full width at half maximum (FWHM) of the diffraction peaks.

2.4.7. Atomic force microscopy (AFM)

AFM imaging of CNC and CNC ultra-fine fibers was performed with an Asylum Research MFP-3D atomic force microscope (Santa Barbara, CA). A few drops of the diluted suspension (0.001, w/w%) were deposited onto freshly cleaved mica substrate (Highest Grade V1 Mica Discs, 15 mm, Ted Pella, Inc.) and allowed to dry. Samples were scanned in air at ambient relative humidity and temperature in tapping mode with OMCL-AC160TS standard silicon probes (tip radius < 10 nm, spring constant = 28.98 N/m, resonant frequency = ~310 kHz) (Olympus Corp.) under a 1 Hz scan rate and 512 pixels × 512 pixels image resolution. Image processing, section analysis, and 3D simulation were performed with Igor Pro 6.21 loaded with MFP3D 090909 + 1409. The average heights were determined from AFM height images.

2.4.8. Surface area and porosity measurements

The nitrogen adsorption–desorption isotherms of degassed (35 °C under vacuum for 24 h) samples were measured at 77 K by a surface area and porosity analyzer (ASAP 2020, Micromeritics, USA). Specific surface areas were calculated from the linear region of the isotherms using the Brunauer–Emmett–Teller (BET) equation in a relative P/P_o pressure range of 0.06–0.20. Pore size distributions were derived from the adsorption branch of the isotherms by Barrett–Joyner–Halenda (BJH) method. The total pore volumes were estimated from the amount adsorbed at a relative pressure of P/P_o = 0.98.

3. Results and discussion

3.1. Isolation of cellulose fibers (CFs) from rice straw

Cellulose was successfully isolated from cleaned and dried rice straw powder through a straightforward three-step de-waxing, delignification and hemicellulose (and silica) removing process. The brown color of the rice straw powder reduced with each step of delignification and hemicellulose removal to become pure white. The resultant white product was confirmed to be cellulose by FTIR spectra (Fig. 1). The spectra also clearly verified the sequential and complete removal of lignin (1516 cm^{-1}, aromatic skeletal vibrations) in de-lignification (Fig. 1c) and leaching of hemicellulose

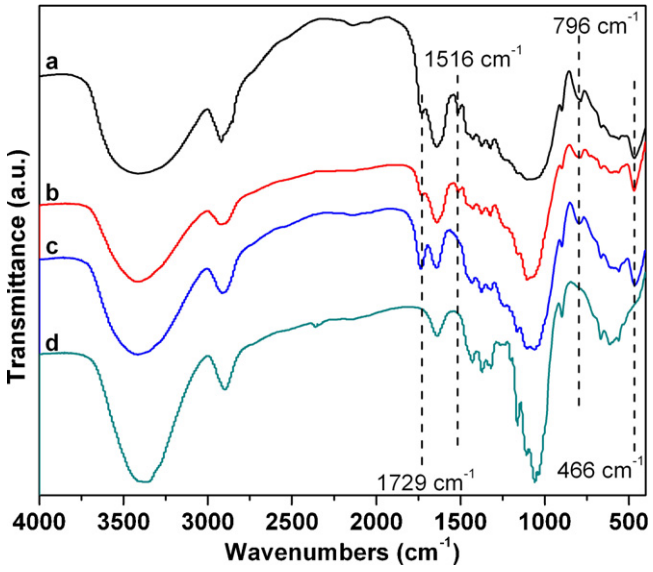

Fig. 1. FTIR of rice straw during isolation process following: (a) water washing, (b) de-waxing, (c) de-lignification, and (d) removal of hemicellulose and silica.

(1729 cm^{-1}, carbonyl stretching) and silica (796 and 466 cm^{-1}, Si–O–Si stretching) in the third step (Fig. 1d), in isolating pure cellulose from rice straw. The total yield of cellulose from rice straw is 36.39%. This yield is close to the values reported in the literature (Hessien et al., 2009), manifesting the high effectiveness of this three-step process for isolating cellulose from rice straw.

SEMs (Fig. 2A) showed the isolated cellulose to be mostly in the form of fibers with an average diameter of 4.5 ± 1.3 μm. These cellulose fibers (CFs) appeared anisotropic under crossed-polars of an optical microscope (Fig. 2B), revealing the high orientation of cellulose chains along the fiber axes. Moreover, the large pieces consisted multiple well aligned bundles of CFs with clear boundaries, showing potential to be further broken down to individualized CFs with additional means.

3.2. Cellulose nanocrystals (CNCs)

The relatively low 45 °C temperature chosen for acid hydrolysis has shown to be more controllable than those carried out at higher temperatures such as 65 °C (Dong, Revol, & Gray, 1998). The hydrolysis lasted for 30 and 45 min and the corresponding products were referred to as CNC30 and CNC45, respectively. The yields for CNC30 and CNC45 lowered with increasing lengths of hydrolysis and were 6.43% and 4.83% of the starting pure rice straw cellulose, respectively. Both CNC30 and CNC45 appeared as individual, isotropically dispersed rod-like crystals in TEM from air-drying of dilute CNC suspensions (0.005, w/w%) droplets on the carbon-coated TEM grids (Fig. 3a and b).

The lengths and widths of CNC30 and CNC45 determined from more than 200 CNCs in TEM images are presented by their ranges and distributions (Fig. 3). The CNC30 ranged from 10 to 65 nm in width (Fig. 3d) and 50 to 700 nm in length (Fig. 3c), averaged 30.7 nm (31%CV) in width and 270 nm (39%CV) in length. In contrast, CNC45 had a much smaller mean width of 11.2 nm (32%CV) and mean length of 117 nm (33%CV), with widths ranging from 4 to 26 nm (Fig. 3f) and lengths from 40 to 260 nm (Fig. 3e). On the average, the width and length of CNC45 were 36% and 43% of those of CNC30, respectively. The aspect (length to width) ratios of CNC30 and CNC45 were calculated to be 8.8 and 10.5, respectively. The aspect ratios of CNC30 and CNC45 are not as much different from each other as their actual dimensions, but lower than those reported on CNCs from other cellulosic sources, such as cotton

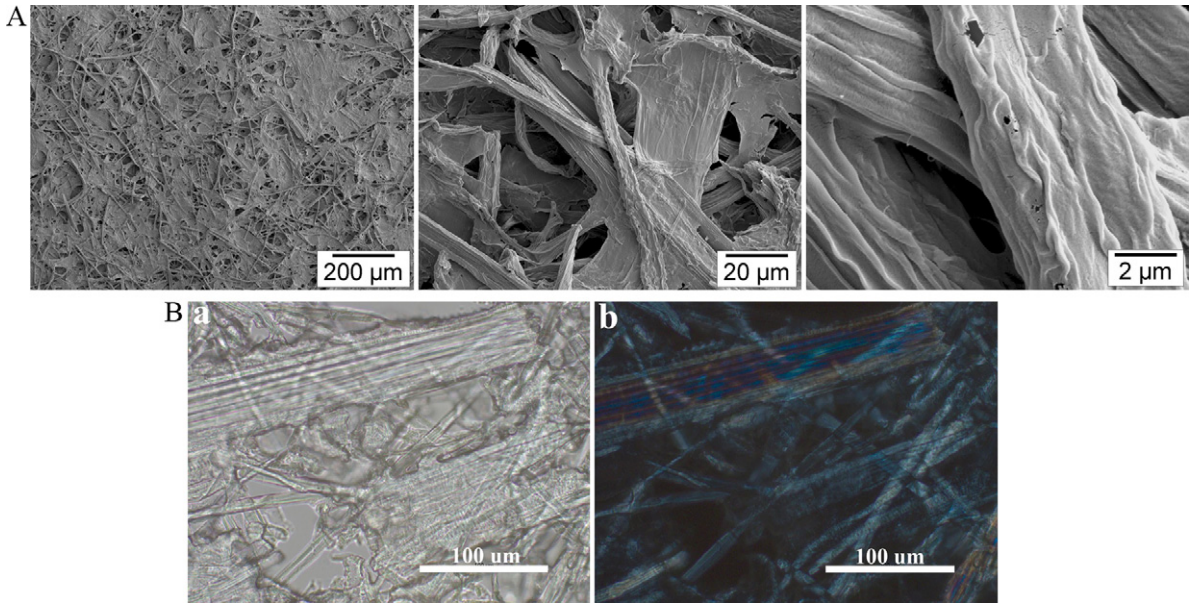

Fig. 2. Cellulose fibers isolated from rice straw: (A) SEM images; (B) optical microscopy: (a) without and (b) under crossed-polars.

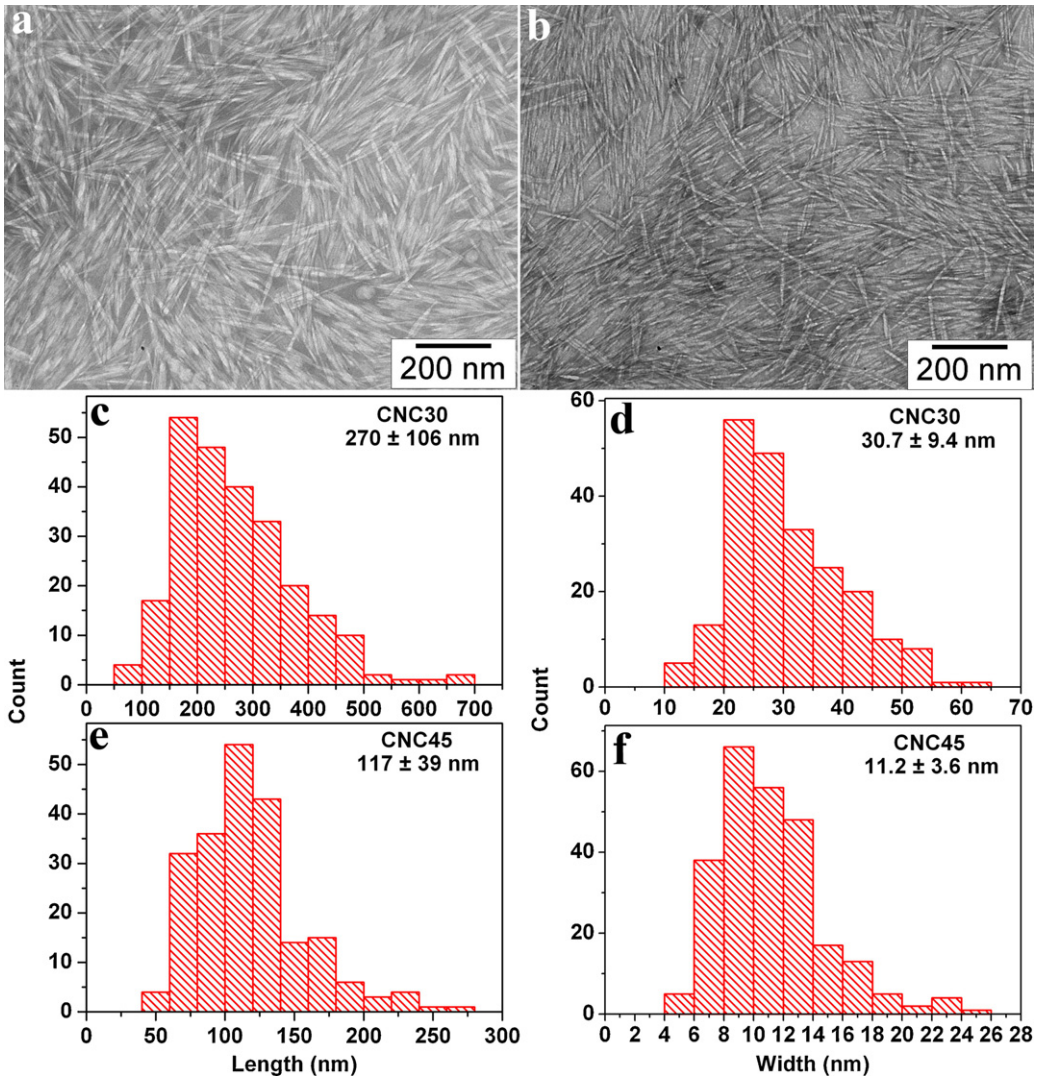

Fig. 3. TEM images of CNCs from acid hydrolysis (64–65% H_2SO_4, 45 °C) of cellulose fibers for: (a) 30 min (CNC30) and (b) 45 min (CNC45); and their length (c and e) and width (d and f) distributions.

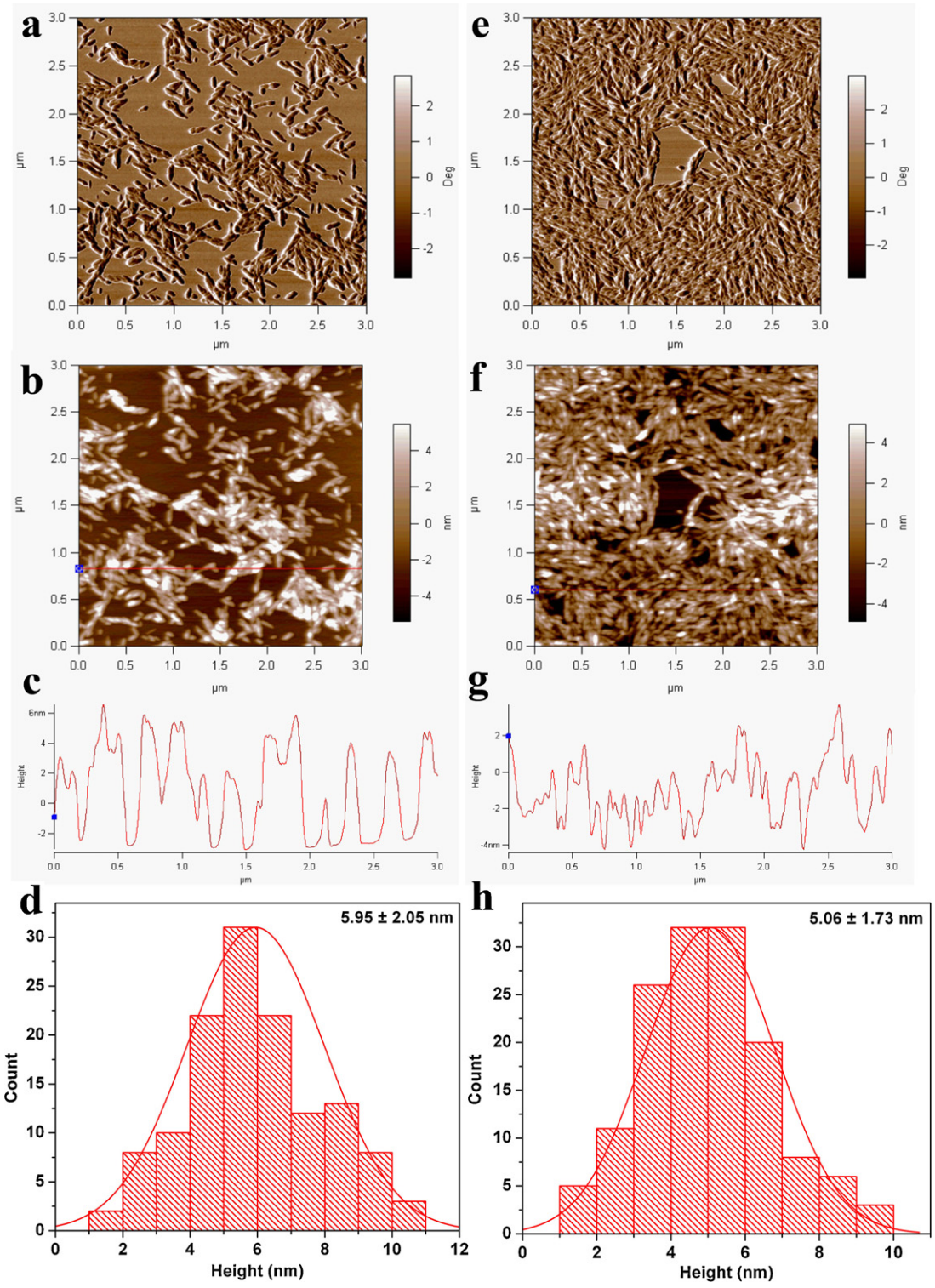

Fig. 4. AFM of CNC30 (a–d) and CNC45 (e–h): phase images (a and e), height image (b and f), height profiles at line positions (c and g) and height distributions (d and h).

(15) (Qi et al., 2009), wood (35–38)(Roman & Gray, 2005), ramie (25–42)(Habibi et al., 2008), sisal (43) (Siqueira et al., 2010), bacteria (60–80)(Olsson et al., 2010) and tunicate (251–493)(Iwamoto et al., 2009).

The dimensions of CNCs were further elucidated by AFM of air-dried highly diluted suspensions (0.001, w/w%) deposited on freshly cleaved mica surfaces (Fig. 4). AFM phase images collected under the tapping mode showed typical distributions of both CNC 30 (Fig. 4a) and CNC45 (Fig. 4e) with the latter being more numerous as expected from its much smaller dimensions at a similar concentration. The height profiles of both CNCs (Fig. 4c and g) are similar, ranging from 1 to 11 nm, with mean heights of 5.95 nm (34%CV) (Fig. 4d) and 5.06 nm (34%CV) (Fig. 4 h) for CNC30 and CNC45, respectively. The much smaller thickness than their corresponding widths of 30.7 and 11.1 nm, showed these CNCs to be flat at 5:1 and 2:1 width-to-thickness ratio for CNC30 and CNC45,

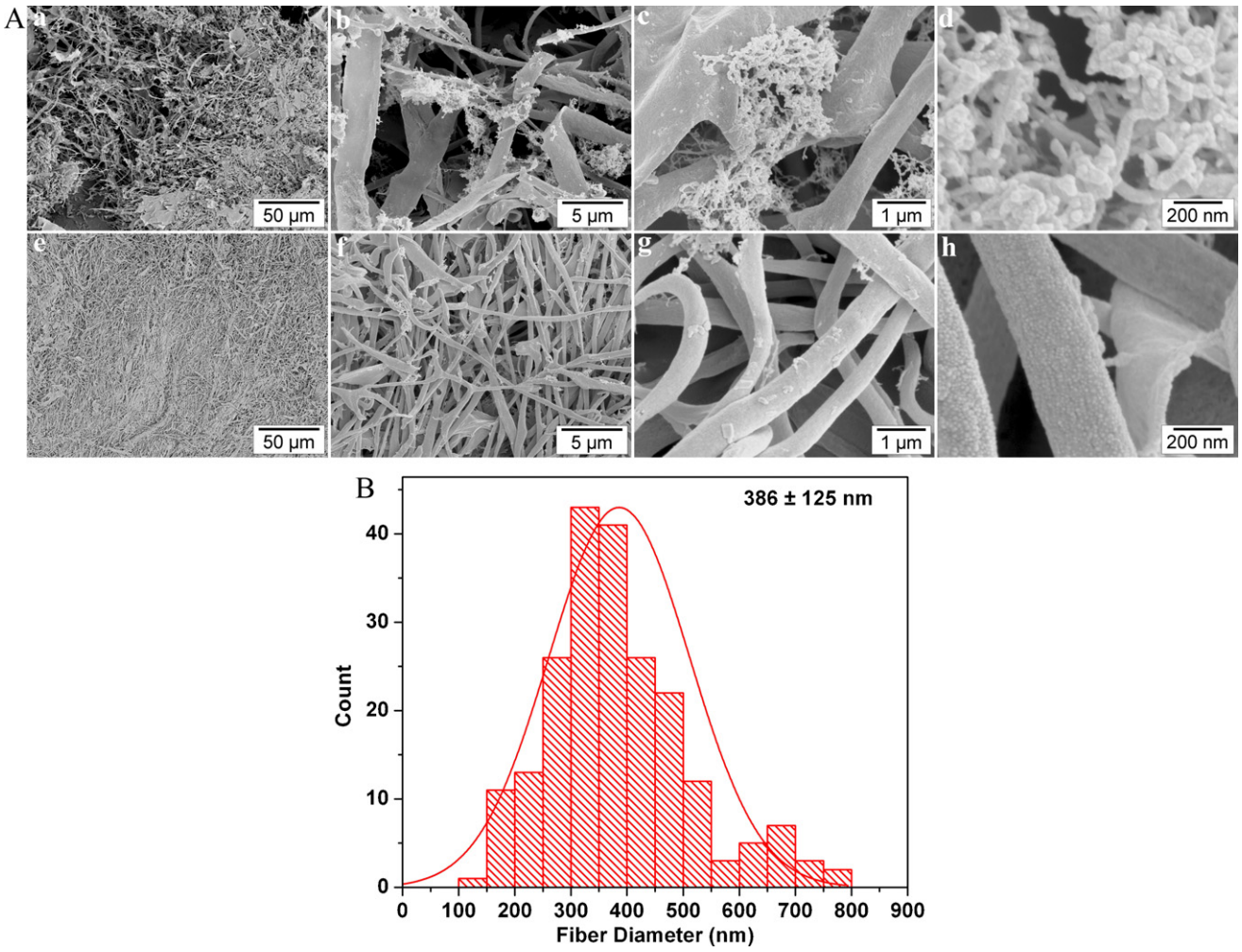

Fig. 5. (A): SEM images of self-assembled products from: (a-d) CNC30 and (e-h) CNC45; (B): diameter distribution of self-assembled ultra-fine fibers of CNC45.

respectively. Although very different in widths, lengths and aspect ratios than CNCs from other sources, the thickness of rice straw CNCs is in the same range as those reported for wood pulp (4.3 nm) (Jiang et al., 2010; Lahiji et al., 2010), cotton (7.3 nm) (Elazzouzi-Hafraoui et al., 2008), and tunicate (8.4 nm) (Iwamoto et al., 2009).

3.3. Cellulose ultra-fine fibers

Very dilute aqueous CNC suspensions, approximately 0.06 wt% CNC, were quickly frozen by adding liquid nitrogen, then freeze–dried. The freeze–dried rice straw CNC products were fluffy. The white fluffy fibrous product from rice straw CNCs had very different appearance than the flaky clumps of cotton CNCs freeze–dried under the same conditions (Lu & Hsieh, 2009, 2010). The SEM images of freeze–dried products from CNC30 and CNC45 showed both to be mostly fibrillar, but different upon closer examination (Fig. 5). Both CNC30 and CNC45 have shown to self-assemble into long fibrous forms with much narrower fiber widths than the 4.5 μm width of originally isolated CFs from rice straw (Fig. 2A). Interestingly, CNC45 self-assembled into mainly sub-micrometer wide ultra-fine fibers (Fig. 2A, e–h) while CNC30 assembled into mostly micrometer wide ribbons with clusters of randomly stringed together CNCs (Fig. 2A, a–d). The ribbons from CNC30 had greatly varied widths, mostly from 1 μm to nearly 2 μm. The self-assembled ultra-fine fibers from CNC45 had widths ranging from 100 to 800 nm, with majority centering at around 350 nm (Fig. 5B). Based on over 200 measurements from SEM images, ultra-fine fibers from CNC45 had a mean width of 386 (±125) nm, 35 times of those of CNC45 (11.2 ± 3.6 nm). Furthermore, ends were not prevalent among fibers assembled from either CNC30 or CNC45, showing the lengths of these self-assembled fibers from CNC30 to be tenths of micrometers and those from CNC45 in hundreds of micrometers.

This intriguing self-assembling behavior of CNCs into fibrillar forms has not been reported on CNCs from other sources and is therefore of great interest to be further characterized in terms of CNC distribution and orientation within the ultra-fine fibers. High resolution SEM showed the fiber surfaces to be highly particulated (Fig. 5A(h)) whereas TEM, usually versatile in revealing internal structures, showed little contrast, indicating a lack of clear internal structure (Fig. 6a). Since the necessary gold sputtering for SEM may mask surface features and high beam intensity in TEM can cause fiber damage, electron microscopy was not capable of offering specifics on the organization of CNCs in these fibers.

The ultra-fine fibers assembled from CNC45 were examined by an AFM scanning probe microscope that employs only moderate mechanical force and requires no sputter coating. The AFM phase image showed alignment of long CNC bundles with undulated surfaces along the fiber axis (Fig. 6b). The corresponding line section analysis of the height image (Fig. 6c) showed a peak fiber height of 412 nm, comparable to the average fiber diameter (386 ± 125 nm) calculated from the SEM images. These fiber height and width val-

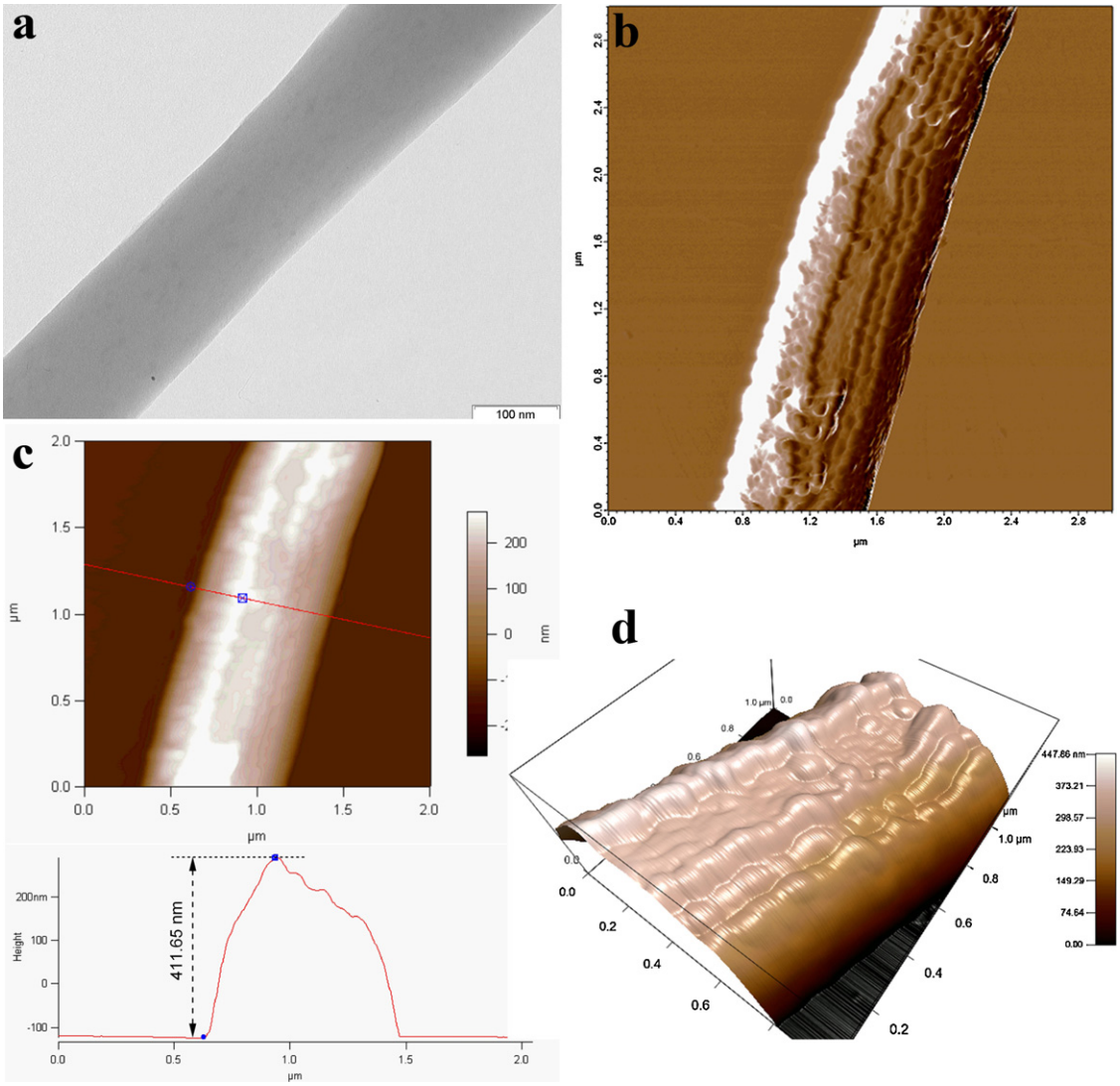

Fig. 6. TEM (a) and AFM (b-d) images of self-assembled ultra-fine fibers of CNC45: phase image showing axially oriented bundles aligning along the fiber axis (b); height profile across fiber width at line position (c); and 3D images showing surface topographies (d).

ues confirmed the essentially cylindrical cross-sectional shape of the CNC45 self-assembled fibers. The larger fiber width shown in Fig. 6c is due to tip broadening effect, common in AFM (Goetz et al., 2010). The 3D image of the height data by Igor Pro software (Fig. 6d) clearly showed the undulated surfaces of the long CNC bundles to be well aligned along the axis direction of the ultra-fine fibers.

The surface areas and porosities of the self-assembled ultra-fine fibers were measured by nitrogen adsorption–desorption method at 77 K (Fig. 7A). Fibers from both CNCs exhibited type II isotherms with nearly reversible loops, indicating their non-porous or macroporous nature. The type II isotherm is also characterized by unrestricted monolayer-multilayer adsorption at high P/P_o as seen in Fig. 7A. The Brunauer–Emmett–Teller (BET) surface area of ultra-fine fibers from CNC45 is 27.625 m^2/g, 3 times of those from CNC30 (8.922 m^2/g). The higher specific surface of fibers assembled from CNC45 is mainly attributed to the smaller fiber sizes than that of flat ribbons from CNC30. Furthermore, both have very low cumulative pore volumes, i.e., 0.025 cm^3/g for CNC30 and 0.084 cm^3/g for CNC45, indicating the closely aligned and tightly bound building elements CNCs via strong hydrogen bonds, leaving little interfacial spaces. The low pore volume results agree well with the observations from SEM, TEM and AFM.

XRD measurements for CFs as well as the self-assembled CNC30 and CNC45 showed similar diffraction patterns with three diffraction peaks at $2\theta = 14.7^\circ$, 16.4°, and 22.6° (Fig. 7B), characteristic of cellulose I crystal (Jiang et al., 2010; Li & Renneckar, 2011; Qi et al., 2009; Siqueira et al., 2010). The crystallinity index (CrI) for CFs was 61.8% whereas those for the self-assembled CNCs were significantly higher at 86.0% and 91.2% for CNC30 and CNC45, respectively. The average crystallite size of CFs was 4.42 nm and those for the self-assembled CNC30 and CNC45 were 7.36 nm and 8.33 nm, respectively. The increased crystallite sizes of the self-assembled CNC30 and CNC45 are believed to mainly reflect the narrowing of the crystallite size distribution with acid hydrolysis. The similar crystallite sizes of CNC30 and CNC45 may also suggest their dimensions to be approaching the elemental crystallite size of rice straw cellulose. The significantly higher crystallinity of the self-assembled CNC30 and CNC45 than the original CFS is attributed mainly to the removal of amorphous cellulose. Furthermore, it implies that, during self-assembling, these CNCs not only aligned well with each other but also form better organized and

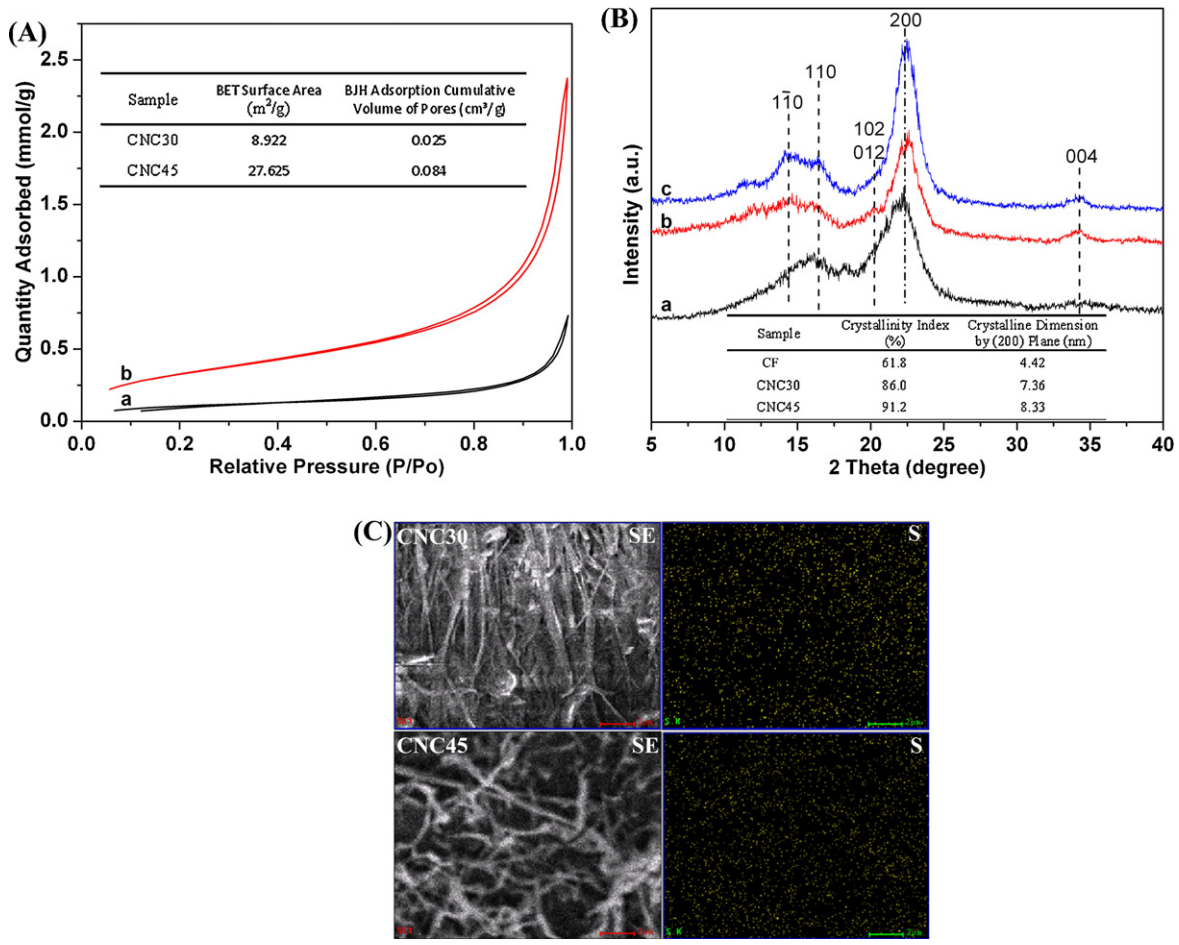

Fig. 7. (A): Nitrogen adsorption–desorption isotherms at 77 K of self-assembled products from: (a) CNC30 and (b) CNC45. The inset table lists the BET surface area and BJH cumulative pore volume calculated from the adsorption branch of each isotherm; (B): XRD of: (a) CFS and self-assembled products from (b) CNC30 and (c) CNC45. Crystallinity index (CrI) and crystalline dimension in the inset table were derived by deconvolution of the XRD peaks; (C): Secondary electron (left) and sulfur mapping (right) of CNCs: (top) CNC30 and (bottom) CNC45.

possibly crystalline interfaces, exceeding the crystalline order in the original CFS. This improved organization and alignment during assembling of CNCs imply their sizes to be more uniform and/or surfaces to be highly ordered to enabling close packing, forming hydrogen bonds between CNCs thus larger and highly crystalline bundles and eventual fibers. That the generation of CNC by acid hydrolysis followed by their self-assembling into fibril structures retain the same cellulose I crystalline structure is expected.

The introduction of sulfate groups onto CNC surfaces from sulfuric acid hydrolysis of rice straw cellulose was confirmed by sulfur mapping (Fig. 7C). These negatively charged sulfate groups on the CNC surfaces provide electrostatic repulsion among individual CNCs to form homogenous and stable aqueous suspensions, as observed by others (Jiang et al., 2010). The sulfur contents of rice straw CNCs are, however, relatively low. CNC30 contains 0.18 at% sulfur while CNC45 has much less sulfur of 0.05 at%. This much less sulfur of CNC45 may explain the more uniformly assembled fibers than those observed on CNC30. This is consistent with our previous report that cotton CNCs with 0.85 at% sulfur freeze–dried into large flakes under the same conditions (Lu & Hsieh, 2010), possibly ascribed to the more highly charged surface sulfate groups. Additionally, the CNC dimensions may also play important role in their self-assembly behaviors. Rice straw CNCs have relatively lower aspect ratios (Fig. 3) and thickness (Fig. 4) than CNCs from other sources (Olsson et al., 2010; Siqueira et al., 2010). For instance, cotton CNCs are similar in width as CNC45, but two to three times longer. Cotton CNCs with higher aspect ratios and higher surface charges did not self-assemble into fibers (Lu & Hsieh, 2010). The self-assembly of the smaller CNC45s into more uniform ultra-fine fibers could be a combination of strong interfacial attraction (low charge density, high hydrogen bonding) and compacted geometry (smallness in size and aspect ratio) and possibly crystallization as shown by the XRD data. This intriguing self-assembling behavior of rice straw CNCs is being further investigated.

These self-assembled ultra-fine fibers from rice straw CNC45 are highly hydrophilic and form a suspension easily by simple hand-shaking. Microscopic observation of a drop of the suspension on glass slide showed these ultra-fine fibers remained intact (Fig. 8a), a clear indication of structural stability. Following prolonged mechanical stirring (300 rpm, 10 h) of the suspension, the fibrous structure also remained unchanged (Fig. 8b), demonstrating extraordinary structural stability of the ultra-fine fibers. This outstanding structural integrity in aqueous media and under prolonged mechanical stirring is attributed to the tight association of the CNCs through the abundant inter-crystal hydrogen bonds, corroborated by the lack of free space between CNC interfaces from the surface and porosity measurements (Fig. 7A) to allow water to penetrate. Furthermore, the observation under crossed-polars (Fig. 8c) revealed that the mechanically stirred samples still

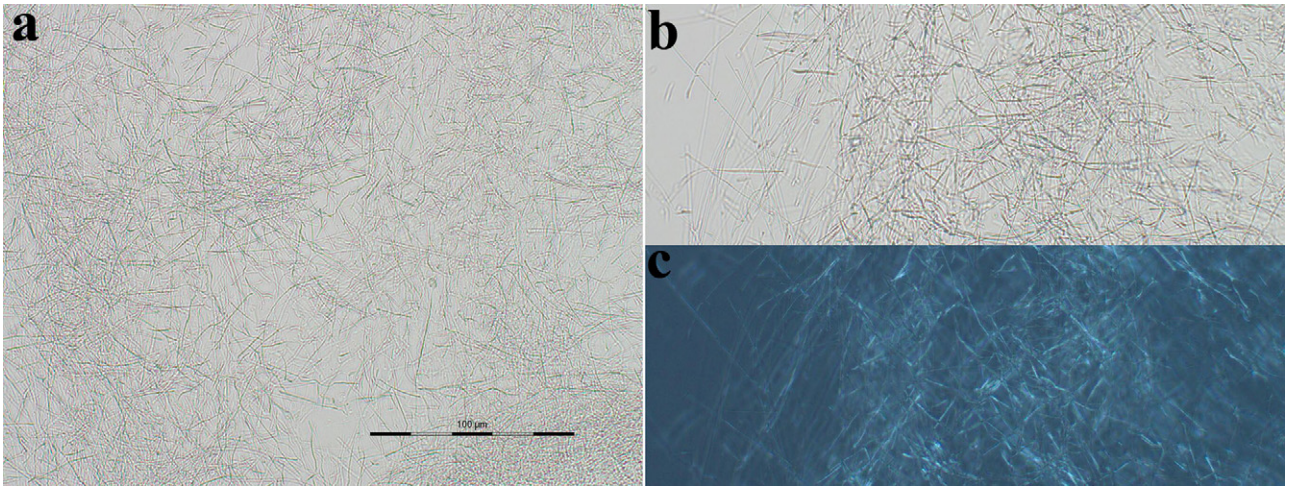

Fig. 8. Optical microscope images, all with 100 μm scale bar,showing the ultra-fine fibers dispersed in water by: (a) hand-shaking and (b,c) mechanically stirred for 10 h at 300 rpm. The image under crossed-polars (c) clearly shows these ultra-fine fibers to be anisotropic, indicative the highly oriented CNCs along the fiber axes.

retained their anisotropic nature, showing no damage or deformation of the fibers. It should be noted that these assembled fibers could be re-dispersed into aqueous CNC suspensions by sonication and reassembled under the same freeze–drying condition.

4. Conclusions

Pure cellulose was isolated from rice straw by an effective three-step process: de-wax by 2:1 v/v toluene/ethanol extraction, de-lignification by prolonged 1.4% acidified $NaClO_2$ dissolution (70 °C for 5 h), and removal of hemicellulose and silica by 5% KOH swelling (24 h) and reaction (90 °C for 2 h), to a yield exceeding 36%. The white cellulose fibers (CFs), with a mean diameter of 4.5 (±1.3) μm, appeared highly anisotropic under polarized microscope. Acid hydrolysis (64% H_2SO_4, 8.75 mL/g, 45 °C) of the pure rice straw cellulose fibers for 30 and 45 min yielded 6.43% and 4.83% cellulose nanocrystals (CNCs), respectively. CNC30 were wider (30.7 nm wide, 5.95 nm thick) and longer (270 nm long) than CNC45 (11.2 nm wide, 5.06 thick and 117 nm long). Most intriguing self-assembly behavior was observed with both CNCs from freeze–drying of their dilute suspensions (0.06 wt%): CNC45 assembled into essentially cylindrically shaped fibers with an 386 nm mean diameter whereas CNC30 formed mostly 1–2 μm wide broad ribbons with some interspersed clusters and strings of nanocrystals. These self-assembled fibers were intriguingly long with estimated lengths in tenths and hundreds of micrometers for CNC30 and CNC45, respectively. Furthermore, AFM observations showed the self-assembled CNC45 ultra-fine fibers contain highly orientated CNCs along the fiber axes. The tightly bound CNCs produced a nonporous or macroporous structure with BET surface area of 8.922 m^2/g and 27.625 m^2/g for CNC30 and CNC45, respectively. The significantly higher crystallinity index (CrI) of the self-assembled CNC30 (86.0%) and CNC45 (91.2%) than the original cellulose fibers (61.6%) suggest uniquely enhanced structural order, possibly crystallization, induced by the freeze–drying process. The outstanding self-assembling behavior of CNC45 was believed to be associated with the low aspect ratio, low and nearly cylindrical lateral dimension and low surface charge. These long, fibrillar structures assembled from rice straw CNCs are highly crystalline, robust and stable under vigorous shaking or stirring in aqueous media, showing unique properties with great promise for advanced materials and functional applications.

Acknowledgement

Financial support for this research by the California Rice Research Board (Project RU-9) is greatly appreciated.

References

Abe, K., Iwamoto, S., & Yano, H. (2007). Obtaining cellulose nanofibers with a uniform width of 15 nm from wood. *Biomacromolecules*, *8*(10), 3276–3278.
Abe, K., & Yano, H. (2010). Comparison of the characteristics of cellulose microfibril aggregates isolated from fiber and parenchyma cells of Moso bamboo (*Phyllostachys pubescens*). *Cellulose*, *17*(2), 271–277.
Ahola, S., Salmi, J., Johansson, L. S., Laine, J., & Osterberg, M. (2008). Model films from native cellulose nanofibrils preparation, swelling, and surface interactions. *Biomacromolecules*, *9*(4), 1273–1282.
Cao, X. D., Habibi, Y., & Lucia, L. A. (2009). One-pot polymerization, surface grafting, and processing of waterborne polyurethane–cellulose nanocrystal nanocomposites. *Journal of Materials Chemistry*, *19*(38), 7137–7145.
de Mesquita, J. P, Donnici, C. L., & Pereira, F. V. (2010). Biobased nanocomposites from layer-by-layer assembly of cellulose nanowhiskers with chitosan. *Biomacromolecules*, *11*(2), 473–480.
Dong, S. P., & Roman, M. (2007). Fluorescently labeled cellulose nanocrystals for bioimaging applications. *Journal of the American Chemical Society*, *129*(45), 13810–13811.
Dong, X. M., Revol, J. F., & Gray, D. G. (1998). Effect of microcrystallite preparation conditions on the formation of colloid crystals of cellulose. *Cellulose*, *5*(1), 19–32.
Dugan, J. M., Gough, J. E., & Eichhorn, S. J. (2010). Directing the morphology and differentiation of skeletal muscle cells using oriented cellulose nanowhiskers. *Biomacromolecules*, *11*(9), 2498–2504.
Elazzouzi-Hafraoui, S., Nishiyama, Y., Putaux, J. L., Heux, L., Dubreuil, F., & Rochas, C. (2008). The shape and size distribution of crystalline nanoparticles prepared by acid hydrolysis of native cellulose. *Biomacromolecules*, *9*(1), 57–65.
Goetz, L., Foston, M., Mathew, A. P., Oksman, K., & Ragauskas, A. J. (2010). Poly(methyl vinyl ether-co-maleic acid)-polyethylene glycol nanocomposites cross-linked in situ with cellulose nanowhiskers. *Biomacromolecules*, *11*(10), 2660–2666.
Habibi, Y., Goffin, A. L., Schiltz, N., Duquesne, E., Dubois, P., & Dufresne, A. (2008). Bionanocomposites based on poly(epsilon-caprolactone)-grafted cellulose nanocrystals by ring-opening polymerization. *Journal of Materials Chemistry*, *18*(41), 5002–5010.
Habibi, Y., Lucia, L. A., & Rojas, O. J. (2010). Cellulose nanocrystals: chemistry, self-assembly, and applications. *Chemical Reviews*, *110*(6), 3479–3500.
Hessien, M. M., Rashad, M. M., Zaky, R. R., Abdel-Aal, E. A., & El-Barawy, K. A. (2009). Controlling the synthesis conditions for silica nanosphere from semi-burned rice straw. *Materials Science and Engineering B-Advanced Functional Solid-State Materials*, *162*(1), 14–21.
Ishii, D., Saito, T., & Isogai, A. (2011). Viscoelastic evaluation of average length of cellulose nanofibers prepared by TEMPO-mediated oxidation. *Biomacromolecules*, *12*(3), 548–550.
Iwamoto, S., Kai, W. H., Isogai, A., & Iwata, T. (2009). Elastic modulus of single cellulose microfibrils from tunicate measured by atomic force microscopy. *Biomacromolecules*, *10*(9), 2571–2576.
Jiang, F., Esker, A. R., & Roman, M. (2010). Acid-catalyzed and solvolytic desulfation of H_2SO_4-hydrolyzed cellulose nanocrystals. *Langmuir*, *26*(23), 17919–17925.
Lahiji, R. R., Xu, X., Reifenberger, R., Raman, A., Rudie, A., & Moon, R. J. (2010). Atomic force microscopy characterization of cellulose nanocrystals. *Langmuir*, *26*(6), 4480–4488.

Li, Q., & Renneckar, S. (2011). Supramolecular structure characterization of molecularly thin cellulose I nanoparticles. *Biomacromolecules*, *12*(3), 650–659.
Lu, P., & Hsieh, Y.-L. (2010). Preparation and properties of cellulose nanocrystals: Rods, spheres, and network. *Carbohydrate Polymers*, *82*(2), 329–336.
Lu, P., & Hsieh, Y. L. (2009). Cellulose nanocrystal-filled poly(acrylic acid) nanocomposite fibrous membranes. *Nanotechnology*, *20*(41), 415604.
Magalhaes, W. L. E., Cao, X., & Lucia, L. A. (2009). Cellulose nanocrystals/cellulose core-in-shell nanocomposite assemblies. *Langmuir*, *25*(22), 13250–13257.
Mahmoud, K. A., Mena, J. A., Male, K. B., Hrapovic, S., Kamen, A., & Luong, J. H. T. (2010). Effect of surface charge on the cellular uptake and cytotoxicity of fluorescent labeled cellulose nanocrystals. *Acs Applied Materials & Interfaces*, *2*(10), 2924–2932.
Okita, Y., Fujisawa, S., Saito, T., & Isogai, A. (2010). TEMPO-oxidized cellulose nanofibrils dispersed in organic solvents. *Biomacromolecules*, 518–522.
Olsson, R. T., Kramer, R. H., Lopez-Rubio, A., Torres-Giner, S., Ocio, M. J., & Lagaron, J. M. (2010). Extraction of microfibrils from bacterial cellulose networks for electrospinning of anisotropic biohybrid fiber yarns. *Macromolecules*, *43*(21), 4201–4209.
Paakko, M., Ankerfors, M., Kosonen, H., Nykanen, A., Ahola, S., Osterberg, M., et al. (2007). Enzymatic hydrolysis combined with mechanical shearing and high-pressure homogenization for nanoscale cellulose fibrils and strong gels. *Biomacromolecules*, *8*(6), 1934–1941.
Peresin, M. S., Habibi, Y., Zoppe, J. O., Pawlak, J. J., & Rojas, O. J. (2010). Nanofiber composites of polyvinyl alcohol and cellulose nanocrystals: Manufacture and characterization. *Biomacromolecules*, *11*(3), 674–681.
Qi, H. S., Cai, J., Zhang, L. N., & Kuga, S. (2009). Properties of films composed of cellulose nanowhiskers and a cellulose matrix regenerated from alkali/urea solution. *Biomacromolecules*, *10*(6), 1597–1602.
Roman, M., & Gray, D. G. (2005). Parabolic focal conics in self-assembled solid films of cellulose nanocrystals. *Langmuir*, *21*(12), 5555–5561.
Segal, L., Creely, J. J., Martin, A. E., & Conrad, C. M. (1959). An empirical method for estimating the degree of crystallinity of native cellulose using the X-ray diffractometer. *Textile Research Journal*, *29*(10), 786–794.
Siqueira, G., Bras, J., & Dufresne, A. (2010). New process of chemical grafting of cellulose nanoparticles with a long chain isocyanate. *Langmuir*, *26*(1), 402–411.
Stephens, C. H., Whitmore, P. M., Morris, H. R., & Bier, M. E. (2008). Hydrolysis of the amorphous cellulose in cotton-based paper. *Biomacromolecules*, *9*(4), 1093–1099.
Sun, J. X., Sun, X. F., Zhao, H., & Sun, R. C. (2004). Isolation and characterization of cellulose from sugarcane bagasse. *Polymer Degradation and Stability*, *84*(2), 331–339.
Uetani, K., & Yano, H. (2011). Nanofibrillation of wood pulp using a high-speed blender. *Biomacromolecules*, *12*(2), 348–353.
Winter, H. T., Cerclier, C., Delorme, N., Bizot, H., Quemener, B., & Cathala, B. (2010). Improved colloidal stability of bacterial cellulose nanocrystal suspensions for the elaboration of spin-coated cellulose-based model surfaces. *Biomacromolecules*, *11*(11), 3144–3151.
Yu, C. T., Chen, W. H., Men, L. C., & Hwang, W. S. (2009). Microscopic structure features changes of rice straw treated by boiled acid solution. *Industrial Crops and Products*, *29*(2–3), 308–315.
Zoppe, J. O., Peresin, M. S., Habibi, Y., Venditti, R. A., & Rojas, O. J. (2009). Reinforcing poly(epsilon-caprolactone) nanofibers with cellulose nanocrystals. *ACS Applied Materials & Interfaces*, *1*(9), 1996–2004.